ACS APPLIED MATERIALS & INTERFACES

Research Article

www.acsami.org

Development of Noncytotoxic Chitosan–Gold Nanocomposites as Efficient Antibacterial Materials

Anna Regiel-Futyra,[†] Małgorzata Kus-Liśkiewicz,*[,‡] Victor Sebastian,[§,∥] Silvia Irusta,[§,∥] Manuel Arruebo,*[,§,∥] Grażyna Stochel,[†] and Agnieszka Kyzioł*[,†]

[†]Faculty of Chemistry, Jagiellonian University, Ingardena 3, 30-060 Kraków, Poland

[‡]Faculty of Biotechnology, Biotechnology Centre for Applied and Fundamental Sciences, University of Rzeszów, Sokołowska 26, 36-100 Kolbuszowa, Poland

[§]Department of Chemical Engineering and Nanoscience Institute of Aragon (INA), University of Zaragoza, 50018 Zaragoza, Spain

[∥]Networking Research Center on Bioengineering, Biomaterials and Nanomedicine, CIBER-BBN, 50018 Zaragoza, Spain

Supporting Information

ABSTRACT: This work describes the synthesis and characterization of noncytotoxic nanocomposites either colloidal or as films exhibiting high antibacterial activity. The biocompatible and biodegradable polymer chitosan was used as reducing and stabilizing agent for the synthesis of gold nanoparticles embedded in it. Herein, for the first time, three different chitosan grades varying in the average molecular weight and deacetylation degree (DD) were used with an optimized gold precursor concentration. Several factors were analyzed in order to obtain antimicrobial but not cytotoxic nanocomposite materials. Films based on chitosan with medium molecular weight and the highest DD exhibited the highest antibacterial activity against biofilm forming strains of *Staphylococcus aureus* and *Pseudomonas aeruginosa*. The resulting nanocomposites did not show any cytotoxicity against mammalian somatic and tumoral cells. They produced a disruptive effect on the bacteria wall while their internalization was hindered on the eukaryotic cells. This selectivity and safety make them potentially applicable as antimicrobial coatings in the biomedical field.

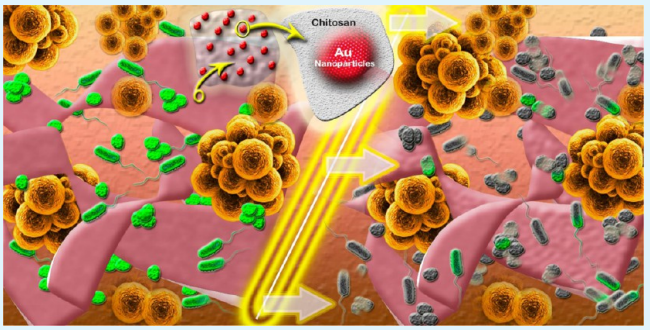

KEYWORDS: *chitosan, gold nanoparticles, composites, antibacterial activity, biocompatibility*

1. INTRODUCTION

Multidrug-resistant (MDR) microorganisms are a major problem for current medicine. Infections caused by resistant bacteria demand prolonged and not always successful treatments that affect negatively mortality and morbidity rates.[1] New resistance mechanisms, as enzymes destroying antibiotics, have emerged, making the new generation of antibiotics virtually ineffective.[2] Patients after organ transplantation or treated for other diseases like cancer, are especially vulnerable to acquire MDR bacterial infections. As an example, almost 170 000 people die each year as a result of tuberculosis caused by MDR bacteria.[3] The mortality rate for patients with MDR infections is about 2 times higher than that for patients with nonresistant bacterial infections.[2] Therefore, there is an urgent need for designing new alternative bactericidal agents.

Nanoscale materials bring new possibilities in the development of effective antimicrobial agents. Several metal nanoparticles (NPs) (e.g., silver, copper, gold) have been synthesized and tested for antimicrobial activity against several pathogenic bacterial strains: *Staphylococcus aureus*, *Echierichia coli*,[4−7] etc. Extensively studied silver and copper nanoparticles arise as potent antimicrobial agents; however, there are many concerns over their cyto- and genotoxicity toward mammalian cells.[8−12] Toxicological studies suggest that those mentioned metallic nanoparticles may cause many unfavorable health and environmental effects. One type of NPs that has recently attracted a lot of attention and, compared to other NPs, exhibits low toxicity is nanoparticulated gold. Due to their chemical stability and easy surface functionalization, AuNPs have been extensively used in drug delivery applications, intracellular gene regulation, bioimaging (as contrast agents), anti-inflammatory therapy and anticancer therapy (photodiagnostic and photothermal therapy).[13−17] Furthermore, the antimicrobial activity of gold nanoparticles has been recently demonstrated,[18−20] although their mechanism of bacterial growth inhibition remains still unclear. Many reports present the bacterial wall damage as the cause of the bacterial cell death. Another hypothesis concerning the mechanism of NPs biocidal activity, focuses on reactive oxygen and nitrogen species (ROS/RNS) generation as a potential cause of bacterial cell damage

Received: August 30, 2014
Accepted: December 18, 2014
Published: December 18, 2014

DOI: 10.1021/am508094e
ACS Appl. Mater. Interfaces 2015, 7, 1087−1099

and death.[21,22] Importantly, the antimicrobial activity strongly depends on the size, shape and surface modifications of AuNPs. For instance, to enhance the antibacterial effect, gold nanoparticles or nanorods were conjugated with photosensitizers and were successfully used to eliminate bacteria by photodynamic antimicrobial therapy.[23,24] All of the enticing properties of AuNPs, mainly noncytotoxic effects toward mammalian cells at the tested concentrations, made them to be perceived as well suited materials for many biomedical applications.[25]

Unfortunately, the reconsideration of gold nanoparticle cytotoxicity has been recently a popular issue. Several reports suggest adverse effects of AuNPs.[26−28] Many multiparametric studies are being conducted in order to elucidate the real nature of nanoparticle−cell interactions. The large variety of approaches makes the data incoherent. Also, many cytotoxicological studies do not take into account the potential interferences of the nanoparticles with the colorimetric assays used.[29,30] However, there are a few common and important assumptions about AuNPs cytotoxicity. It was demonstrated that cell uptake of gold nanoparticles is size, shape, dose, exposure time and cell type dependent.[31−33] The smaller the nanoparticles, the higher the surface to volume ratio and therefore, the number of NP−cellular component interactions increases.[34] Moreover, the decrease in NPs size might be responsible for glutathione level depletion and, consequently, an enhanced cytotoxicity.[35] Still, the size influence on cytotoxicity is not so straightforward. For instance, Mironova et al. have demonstrated that 45 nm AuNPs (20 μg/mL) caused a significant increase in human dermal fibroblasts proliferation doubling time compared to the 13 nm ones (142 μg/mL). Noteworthy, increased doubling time of cells is sometimes faultily addressed as cytotoxicity. Both particle sizes, even though they had different internalization routes, were found to be sequestered inside large vacuoles without showing nuclei penetration.[36] In contrast, Pan et al. reported that 1 and 4 nm gold nanoparticles were the most cytotoxic toward connective tissue fibroblasts, epithelial cells, macrophages and melanoma cells (IC50 ∼ 30−46 μg/mL), whereas 15 nm AuNPs were not toxic at concentrations up to 100-fold higher (up to 6300 μg/mL).[37] Conversely, no difference in cytotoxicity of 10 and 100 nm AuNPs was observed by Hondroulis et al.[38] Furthermore, Connor et al. reported a high rate uptake by human cells (K562, immortalized myelogenous leukemia cell line) with no cytotoxic effect when using 18 nm gold nanoparticles up to 100 μM.[39] Similarly, Shukla et al. presented a discerning report claiming that gold nanoparticles are inert and nontoxic to macrophage cells (RAW264.7) and do not elicit stress-induced secretion of proinflammatory cytokines.[25] Furthermore, inhibition of reactive oxygen and nitric oxide species generation at higher NPs concentration was proven.[25] Another important aspect has been demonstrated, the cytotoxic effect after internalization of gold NPs is often a result of the activity of the coating agent or the gold precursor, e.g., CTAB-capped AuNPs displayed a similar toxicity to CTAB alone, whereas washed CTAB-capped AuNPs were not cytotoxic to human colon leukemia cells (K562) and carcinoma cells (HT-29) (up to 25 μM).[39,40] Going further in the surface modifications, the application of polymer coatings on the surface of Au nanoparticles and nanorods can significantly reduce the cytotoxicity, e.g., by PEG, PAA, PAH, starch modifications.[40−44]

Another important aspect of polymeric−metal composites for biomedical application is their mechanical strength. Addition of an inorganic component to the polymeric film resulted in a decrease of the tensile strength and an increase in the elongation percentage. Mechanical and barrier properties of chitosan films with and without silver nanoparticles were studied by Rhim et al.; after filler addition, the tensile strength increase and water vapor permeability decrease were proven experimentally.[45] Also, Panhius et al. demonstrated the TiO_2 and Ag nanoparticles ability to reinforce mechanical properties and water vapor transmission/water resistance behavior of chitosan films.[46] For both fillers, a significant mechanical improvement of polymeric films was observed (Young's modulus, tensile strength and toughness increase). Importantly, silver nanoparticles induced the enhancement in water swelling.[45,46] Taking those considerations into account, we suggest that the incorporation of chitosan films with gold nanoparticles may induce similar changes in the properties of the resulting films.

Herein we present innovative chitosan−gold nanocomposites. For the first time, solid CS-AuNPs films were carefully analyzed in terms of physicochemical properties and biological activity. Chitosan, a biocompatible carbohydrate polymer, has been used as a reducing and stabilizing agent in a green-synthesis of metal NPs.[47,48] A tremendous advantage of chitosan is its biocidal activity against bacteria, yeast, mold and simultaneous noncytotoxic effects toward mammalian cells.[49−52] We explored the physicochemical influence of the polymer properties (average molecular weight and deacetylation degree) with the resulting AuNP characteristics. Antibacterial activity was evaluated according to the European Norm ASTM E2180-07 for polymeric materials, against selected, resistant Gram-positive and negative bacterial strains (*Staphylococcus aureus* and, *Pseudomonas aeruginosa*, respectively).[53] Finally, in view of their potential biomedical application, the cytotoxicity of the prepared nanocomposites was evaluated using two human cell lines: A549 (human lung adenocarcinoma epithelial cell line) and HaCaT (an immortal human keratinocyte).

2. EXPERIMENTAL SECTION

Materials. Chitosan with low/medium/high (CS_L/M/H) average molecular weight (Mw ∼ 369 ± 4; 1278 ± 8; 2520 ± 9 kDa, respectively) was purchased from Sigma-Aldrich and used as received. Chitosan L and M were obtained from chitin of shrimp shells whereas chitosan H was obtained from chitin of crab shells. The deacetylation degree for CS_L/M/H was 86 ± 3%; 89 ± 2%; 85 ± 3%, respectively.[54] Aqueous solutions of acetic acid (99.8% Sigma-Aldrich) were used as the solvent. Gold(III) chloride trihydrate (≥99.9%; 48.5−50.25% Au), sodium hydroxide (anhydrous, ≥98%), thiazolyl blue tetrazolium bromide (98%) and the LDH (lactate dehydrogenase) assay kit were also supplied by Sigma-Aldrich. Dimethyl sulfoxide (DMSO) and methanol were purchased from Chempur. Phosphate-buffered saline (PBS) without Ca and Mg was purchased from PAA The Cell Culture Company. Dulbecco's modified Eagle's medium (DMEM) high in glucose (4.5 g/L) with L-glutamine with and without phenol red was used in cell culturing and was supplied by Thermo Scientific. Materials for bacteria culturing were purchased from BIOMED (broth) and BIOCORP (agar). Sucrose, sodium cacodylate trihydrate (approximately 98 wt %), glutaraldehyde solution (50 wt % in water) and methanol anhydrous 99.8 wt % (Sigma-Aldrich) were used to fix and dehydrate the cells before scanning electron microscopy (SEM) visualization.

Chitosan based Gold Nanoparticle Synthesis. Chitosan flakes were dissolved at 65 °C under stirring in 0.1 M acetic acid to obtain a

DOI: 10.1021/am508094e
ACS Appl. Mater. Interfaces 2015, 7, 1087−1099

1% (w/v) concentration until clear solutions were obtained (~12 h). Chitosan solutions (L, M, H Mw) were heated up to 60 °C using and oil bath and magnetic stirring. Then, gold chloride solutions (1, 2, 5, 10 mM; always in volume ratio CS:$HAuCl_4$ = 5:2) were added dropwise and the prepared mixtures were kept under heating and stirring for 4 h (optimized synthesis time). The color of the mixture was evolving from colorless (a little bit yellowish for CS_L) to pink and purple, indicating gold nanoparticle formation. To simplify further sample nomenclature, a system of abbreviation was used (e.g., L1 where L stands for chitosan with low Mw and 1 for 1 mM initial gold precursor concentration).

Chitosan-Gold Nanocomposite Preparation. Nanocomposites were prepared by a solvent evaporation method. Chitosan L/M/H (1% (w/v)) solutions and chitosan based gold nanoparticles dispersions (25 mL) were poured into Petri dishes (polystyrene, internal diameter 9 cm) and dried in an electric oven (Pol-Eko) at 60 °C until the solvent was completely evaporated. In a second step, chitosan acetate and chitosan acetate–gold nanoparticles were neutralized with 1 wt % NaOH solution and washed with distilled deionized (DDI) water. Neutralized CS_AuNPs films were dried again in the oven and kept in the dark until further use.

Gold Nanoparticle and Chitosan–Gold Nanocomposite Characterization. UV–Vis spectroscopy was used as an analytical tool to track gold nanoparticle formation. UV–vis measurements were carried out in a double beam UV–vis spectrophotometer (PerkinElmer Lambda 35), over a range between 300 and 800 nm. To evaluate the potential detachment of the gold nanoparticles from the chitosan films, 3 × 3 cm pieces of each CS-AuNPs nanocomposite were placed in glass bottles with 30 mL of distilled water and the supernatant spectrophotometrically analyzed over time. The detection was carried out by measuring UV–vis spectra after 2, 6, 24 and 48 h of incubation. Infrared absorption measurements were performed on a Bruker Equinox infrared spectrophotometer. Each spectrum was collected with 2 cm^{-1} resolution in a range 4000–400 cm^{-1}. Transmission electron microscopy (TEM) images of CS_AuNPs suspensions were taken using an FEI Tecnai T20 Microscope. The size distribution of colloidal AuNPs was determined from the enlarged TEM micrographs, using National Instruments IMAQ Vision Builder software, counting at least 200 particles/image. Size-distribution measurements were performed on an FEI Tecnai T20 microscope and a FEI Tecnai G^2 F30 microscope equipped with a cryoholder to avoid damage on the samples (high resolution scanning transmission electron microscopy (STEM) with a high angle annular dark field (HAADF) detector) at LMA-INA-UNIZAR. Gold nanoparticles were then identified by energy dispersive X-ray spectroscopy (EDS). Nanocomposites were fixed in a resin and cut with an Ultramicrotome (Leica EM UC7) equipped with a diamond knife. Thermogravimetric analysis (Mettler Toledo TGA/STDA 851^e) of chitosan–gold films was applied to determine the degradation temperatures of the polymer, moisture content and percentage of inorganic components in the material. Samples were analyzed in Ar atmosphere (gas flow 50 mL/min) in a temperature range between 30 and 850 °C with a heating rate of 20 °C/min. X-ray photoelectron spectroscopy (Axis Ultra DLD 150, Kratos Tech.) was used to evaluate the AuNP dispersion along the film thickness and weight percentage of NPs in the selected composites. The spectra were excited by the monochromatized Al Kα source (1486.6 eV) run at 15 kV and 10 mA.

Cytotoxicity Assay. To determine the cytotoxic activity of the CS_AuNPs dispersions and films, two different cell lines were used in this study: A549 (human lung adenocarcinoma epithelial cell line) and HaCaT (an immortal human keratinocyte). A549 and HaCaT were maintained in high-glucose Dulbecco's modified Eagle's medium (DMEM) with 1% of antibiotics and 1% of fetal bovine serum (FBS). Cells were cultured at 37 °C in 5% CO_2 saturated air. Culture media were replaced every 2 days. Cells were passaged at least once a week. Before the cytotoxicity assay, all nanocomposites were sterilized under UV light for 30 min.

CS_AuNP Dispersions. Cells were seeded in 96-well flat bottom microtiter plates at a density of 1×10^4 cells per well with 200 μL of medium (37 °C, 5% CO_2 atmosphere). After 24 h of culturing, the medium was aspirated out, and cells were washed with phosphate-buffered saline (PBS). Each well was treated with different CS L/M/H_AuNP dispersions at different concentrations, diluted in DMEM with 1% serum and incubated for 24 h (37 °C, 5% CO_2 atmosphere). A549 cell viability was determined by the MTT assay. Briefly, each well was rinsed with PBS and treated with 200 μL of the MTT solution (0.5 mg/mL in DMEM without serum). After 3–4 h of incubation, MTT was reduced into insoluble purple formazan crystals. Crystals were dissolved in DMSO:CH_3OH (1:1). The absorbance was read in a microplate reader (TECAN Infinite 200) at 565 nm. Results obtained for samples compared with untreated cells as a control were presented as a percentage of viable cells. Any potential interference from the nanoparticles was evaluated and ruled out during the assay. For the HaCaT cell line, MTT and LDH assays were performed. To assess the cytotoxicity of the nanocomposites, the potential lactate dehydrogenase leakage into the culture was assessed. LDH is an enzyme existing in the cell cytoplasm, and is released into the cell culture medium after cell film damage. Therefore, leakage of this enzyme to the intercellular compartments is an indicator of cytotoxicity. LDH activity was measured according to the protocol of Chan et al.[55] For the colloid analysis, cells were seeded in a 96-well (AuNPs colloids) microtiter plates, at a density of 5×10^4 cells/well. Cells were allowed to attach for 24 h and were treated with NP based colloids and incubated another 24 h. Absorbance (at 500 nm) was recorded using a microplate spectrophotometer (Tecan), and the results were presented as a percentage compared to the control values. Each experiment was performed in triplicate and repeated three times.

CS_AuNP Films. A special method to evaluate the cytotoxicity of the nanocomposites was developed in order to obtain reliable and reproducible results. Colloids of CS L/M/H_AuNPs (1, 2, 5 10 mM) after the synthesis were poured into 12-well plate (each sample in three wells). As control, pure CS L/M/H solutions were poured into wells and dried in an electric oven at 60 °C for ~3 h. After film formation, films were neutralized with 1 wt % NaOH and washed with deionized water. Before the cytotoxicity assay was conducted, films were sterilized under UV lamp (30 min). Each well with the corresponding sample was treated with 1 mL of cell suspensions in DMEM enriched with 1% serum (3×10^5 cells/well) and incubated for 24 h (37 °C, 5% CO_2 atmosphere). Cell viability was determined by the MTT/LDH assay. Due to the fact that films could absorb medium with cells and that some of the viable cells were not adhered strongly enough to the support, the PBS washing step was omitted. MTT solution was poured directly to the wells without removing the DMEM.

Chitosan/Gold Nanocomposites Antibacterial Activity Determination. *Bacterial Cultures.* Bacterial strains (*S. aureus* ATCC 25923 and *Pseudomonas aeruginosa* ATCC 27853) were maintained in enriched tryptone soy broth (TSB, BIOMED) and kept at 4 °C. In the preparation of initial culture for antimicrobial test of CS and CS-AuNPs films, 10 μL of bacteria was transferred and inoculated into 10 mL of tryptone soy broth medium (TSB, BIOMED) and incubated at 37 °C for 18–24 h to obtain ~10^9 colony forming units (CFU)/mL. Enriched agar (BIOCORP) was used for seeding plates preparation and initial culture for bactericidal tests preparation. The buffer solution employed for dilutions was phosphate buffered saline (PBS), prepared in a 1:1.2:7.2:40:5000 weight proportion of KCl, KH_2PO_4, Na_2HPO_4, NaCl and distilled water, respectively. Homogenization of solutions was achieved with a vortex. Bacteria cultivation was carried out in a bacteriological incubator (Thermo Scientific, MaxQ 6000). All assays were carried out in a laminar flow hood (Thermo Scientific, MSC Advantage). All materials were sterilized prior to use in an autoclave (Prestige Medical, Classic) at 121 °C during 20 min.

Antimicrobial Activity Determination. To evaluate the antibacterial activity of CS_AuNP nanocomposites in a direct contact form, the ASTM E2180-07 standard method was applied (method for determining the antimicrobial effectiveness of agents incorporated into polymeric surfaces). Pure chitosan films (3 × 3 cm squares) were used as controls. After 24 h of incubation, bacteria colonies were counted and colony forming units were calculated (CFU/mL). The damage and potential rupture in the bacterial cell walls during the

DOI: 10.1021/am508094e
ACS Appl. Mater. Interfaces 2015, 7, 1087–1099

exposure to the chitosan−gold nanocomposites were visualized by SEM (Tescan Vega3 LMU). Detailed information about antibacterial test procedure is available in the Supporting Information.

3. RESULTS AND DISCUSSION

It has been previously demonstrated that an environmentally-friendly synthesis can be applied for the preparation of gold nanoparticles with chitosan acting as both reducing and stabilizing agent.[56] Following this approach, we prepared in situ colloidal gold nanoparticles by direct tetrachloroauric acid reduction in chitosan solutions at 60 °C. To study the influence of the polymer properties on the resulting AuNP characteristics, for the first time, three different chitosan forms were used varying their average molecular weight and deacetylation degree. A dependence of the gold concentration with the color of the resulting dispersions after nanoparticle formation was observed (Figure 1A). Clearly, the higher gold precursor initial concentration, the more intense the color of the subsequent colloid. The electrostatic attraction between positively charged amino groups of the polymeric chains and the negatively charged gold ions ($AuCl_4^-$) results in gold reduction and NP stabilization.[57] Colloidal AuNP suspensions were afterward used for the fabrication of films. Figure 1B shows the resulting CS-AuNP films.

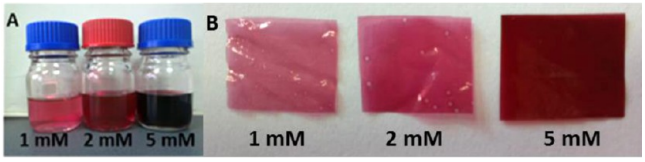

Figure 1. (A) Chitosan based gold nanoparticle colloids after synthesis (1, 2 and 5 mM gold precursor initial concentration, respectively); (B) photographs of chitosan−gold films with different AuNP loadings (1, 2 and 5 mM, respectively).

UV−Vis Spectroscopy. Due to the localized surface plasmon resonance (SPR) effect coming from the excitation of the conduction electrons in the metals, the progress of the AuNP synthesis was tracked by using UV−Vis spectroscopy. The measurements were conducted simultaneously during 8 h for the CS L/M/H AuNPs (1 mM precursor) synthesis (Figure 2A−C).

All spectra show the SPR extinction band at around ∼525 nm, characteristic for spherical gold nanoparticle formation.[58,59] The SPR band appears due to the common excitation of the nanoparticle free electrons. An exponential-decay Mie scattering profile with decreasing photon energy is clearly observable. After 4 h of synthesis, the plasmon peaks remained unaltered, indicating that the reaction was completed after that time which also supports the AuNP formation. The intensity of SPR band increases with the reaction time. In each case a progressive enhancement in the SPR band intensity can be observed, which indicates a progress in the gold reduction process and an increase in the concentration of gold nanoparticles. All of the measurements were concentration normalized. UV−vis spectra were recorded for all of prepared samples: CS_L/M/H_1/2/5 mM AuNPs (Figure2D−F) after the synthesis ended. The stability of gold nanoparticles was confirmed by measuring the spectra after 48 h and after several weeks of synthesis (data not shown). At each concentration, the intensity of the SPR band for AuNPs based on CS H is the lowest, which indicates that the reduction rate is the lowest as well. This result can be supported by the lowest deacetylation degree (DD) value (the less free amino groups available for gold ion coordination and reduction, the lower yield of reduction).[54]

Transmission Electron Microscopy (TEM, Size Statistics). TEM analysis of the CS-AuNPs (1, 2 and 5 mM gold precursor) colloids was used to assess the shape and size distribution of the as-prepared nanoparticles (Figure 3). Micrographs revealed the formation of mainly spherical shaped gold particles. Statistical analysis of the NP sizes based on the obtained micrographs is also presented as an inset. The smallest

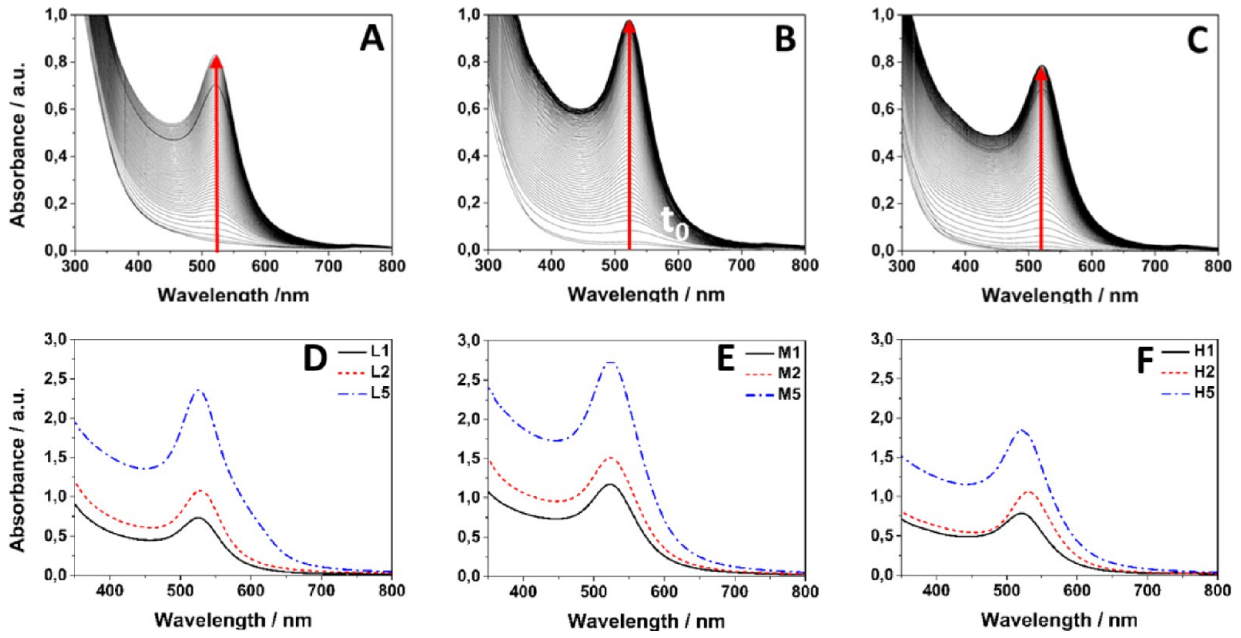

Figure 2. UV−vis absorption spectra for CS_L (A), CS_M (B), CS_H (C) based AuNP synthesis progress (1 mM precursor). Spectra were also collected after synthesis for all gold initial concentrations: CS_L (D), CS_M (E), CS_H (F).

DOI: 10.1021/am508094e
ACS Appl. Mater. Interfaces 2015, 7, 1087−1099

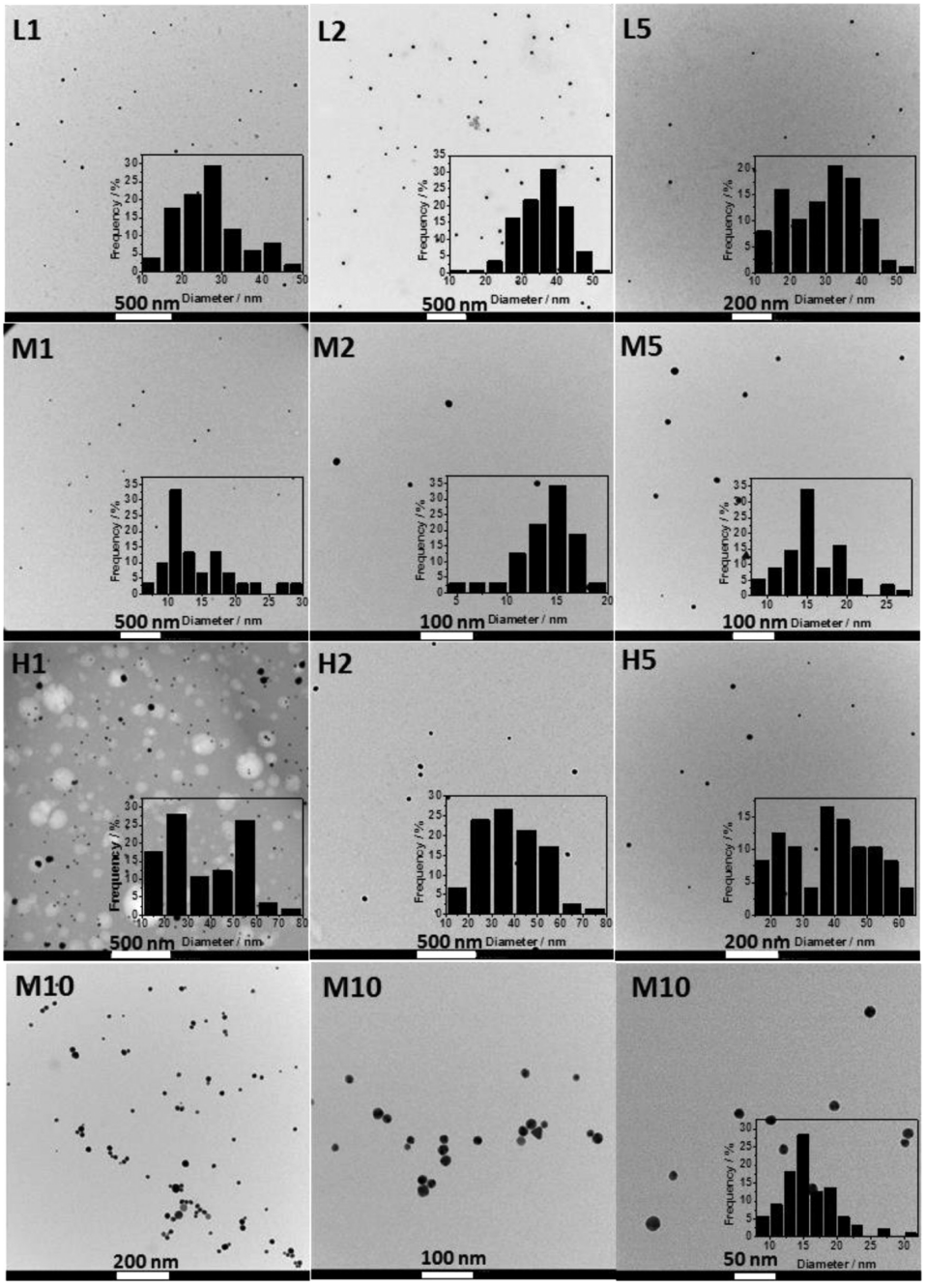

Figure 3. TEM pictures for CS_L/M/H_AuNPs (colloids) based on different gold precursor concentrations used in the synthesis (e.g., M1, M2, M5 and M10 stands for 1, 2, 5 and 10 mM, respectively).

and the narrowest size distribution was obtained for chitosan with the average molecular weight and the highest deacetylation degree at each gold precursor concentration tested (CS_M).

Synthesis with the highest gold initial concentration (10 mM) was additionally performed for the CS_M. The sample consists of nanoparticles with an average diameter of 16 ± 4 nm. In Table 1, the statistical average sizes for all of the samples are listed. Importantly, the smallest particles, at each gold concentration level, were obtained for CS_M.

Using high resolution TEM and contrasting the polymeric matrix using phosphotungstic acid on the M10 colloid, a chitosan halo around the particles can be observed (Supporting Information), which confirms the strong interactions between the polymer and the noble metal surface.

Table 1. Average AuNP Sizes Depending on the Gold Precursor Initial Concentration

	gold nanoparticle sizes/nm		
gold precursor initial concentration/mM	CS_L	CS_M	CS_H
1	26 ± 8	14 ± 5	38 ± 16
2	35 ± 7	14 ± 3	37 ± 13
5	29 ± 10	16 ± 5	36 ± 14
10		16 ± 4	

Transmission Electron Microscopy (TEM) CS_AuNPs Nanocomposites Analysis. To get an insight into the uniformity of the AuNP distribution among the nanocomposites, TEM analysis of the films with the lowest gold

DOI: 10.1021/am508094e
ACS Appl. Mater. Interfaces 2015, 7, 1087−1099

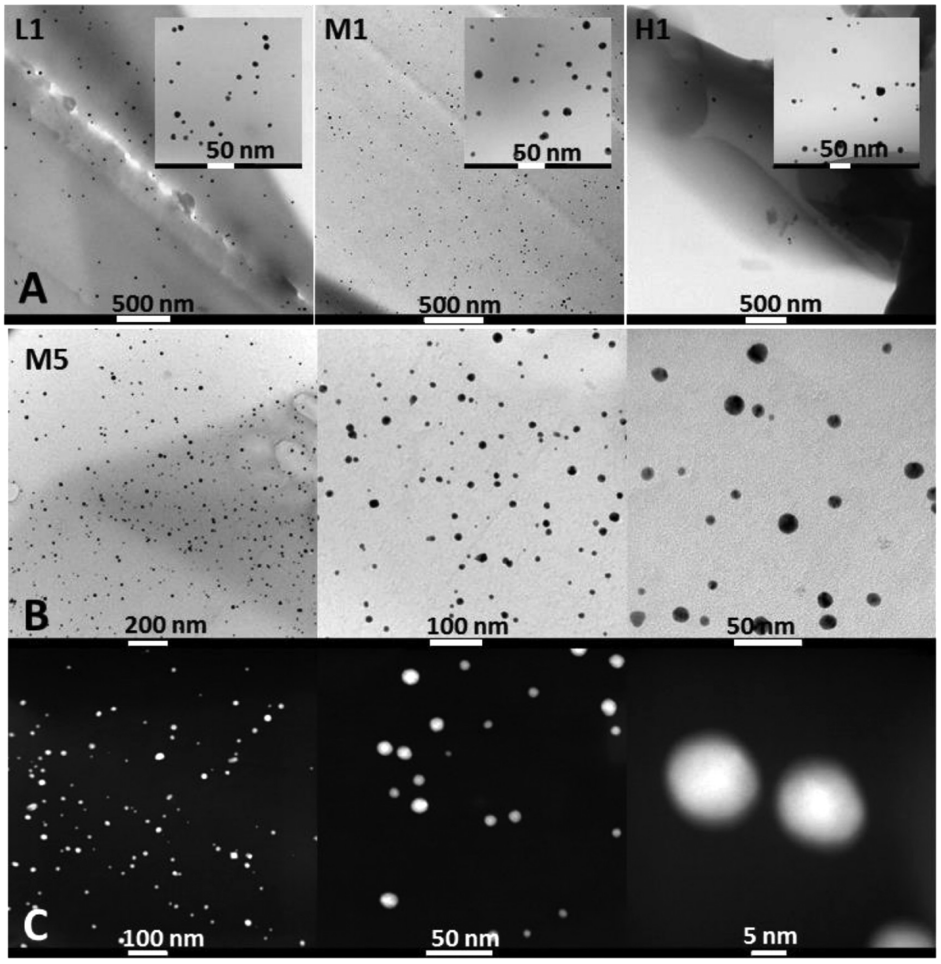

Figure 4. TEM and STEM-HAADF micrographs for L1/M1/H1 nanocomposites (A) and M5 (B and C) nanocomposite reveals a proper gold nanoparticles distribution across the film.

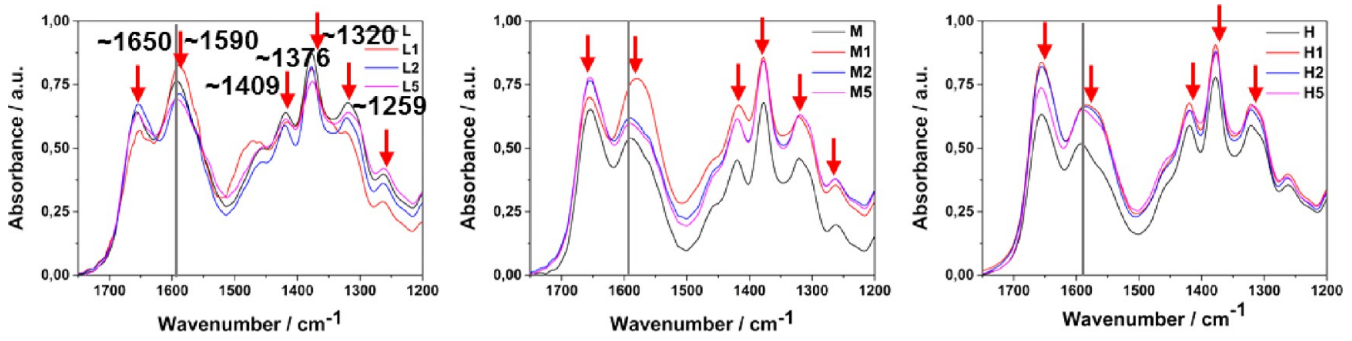

Figure 5. FTIR spectra of pure chitosan films (L/M/H) and their nanocomposites with increased gold NP content.

content was performed. The most uniform AuNP distribution was observed for CS_M based samples (Figure 4AM1). Unlike M1, unequal layout is apparent for chitosan with the highest molecular weight (H1) where many areas lacking NPs or showing large NP based aggregates are present. Although aggregates were not observed for sample L1, the distribution of nanoparticles is less uniform than for the M1 sample. A homogeneous dispersion of AuNPs was also presented for CS_M samples with higher gold content, thus confirming a high stabilizing potential of chitosan with the medium average molecular weight (Figure 4B). Also, STEM-HAADF micrographs collected for this M5 sample presented gold nanoparticles as bright dots because the contrast is directly related to the atomic number, certifying the gold homogeneity when using chitosan medium based materials (Figure 4C).

Energy dispersive spectroscopy elemental analysis (EDS) was performed to provide evidence of the presence of gold nanoparticles in the nanocomposites (Supporting Information).

Fourier Transform Infrared (FTIR) Spectra Analysis. To confirm the specific interaction of chitosan functional groups with the metal surface FTIR spectra of pure chitosan films (L/M/H) and chitosan−gold nanocomposites were collected. For better interpretation, only the region between 1200 and 1750 cm^{-1} is presented. Figure 5 shows representative spectra with the characteristic vibrational bands of chitosan. A typical chitosan spectrum presents bands at ∼1650 and ∼1590 cm^{-1}

DOI: 10.1021/am508094e
ACS Appl. Mater. Interfaces 2015, 7, 1087−1099

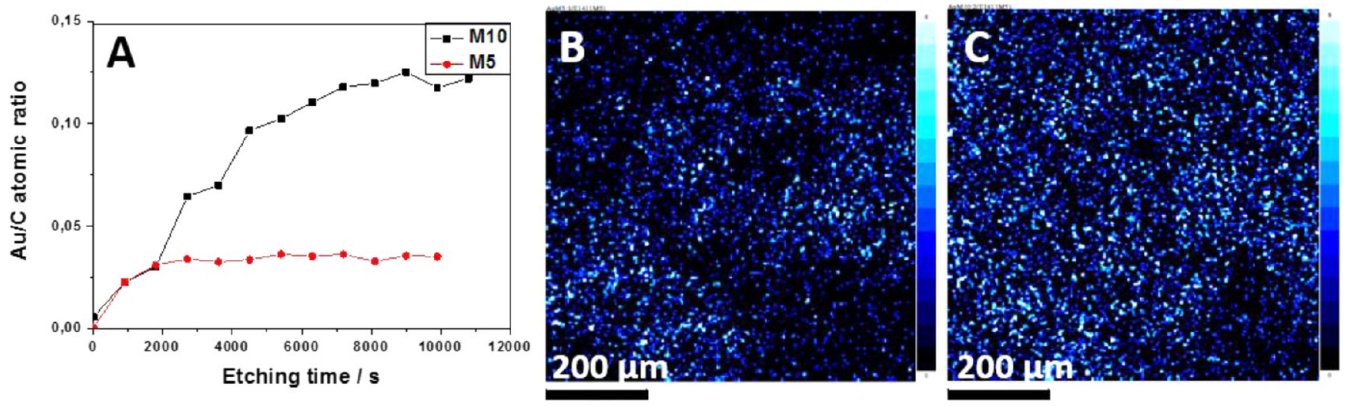

Figure 6. XPS depth profiling results of chitosan−gold films (A); XPS maps of AuNPs distribution for M5. The lighter the blue color, the higher the Au concentration present (B) and M10 (C) film. The lighter the blue color, the higher the Au concentration present.

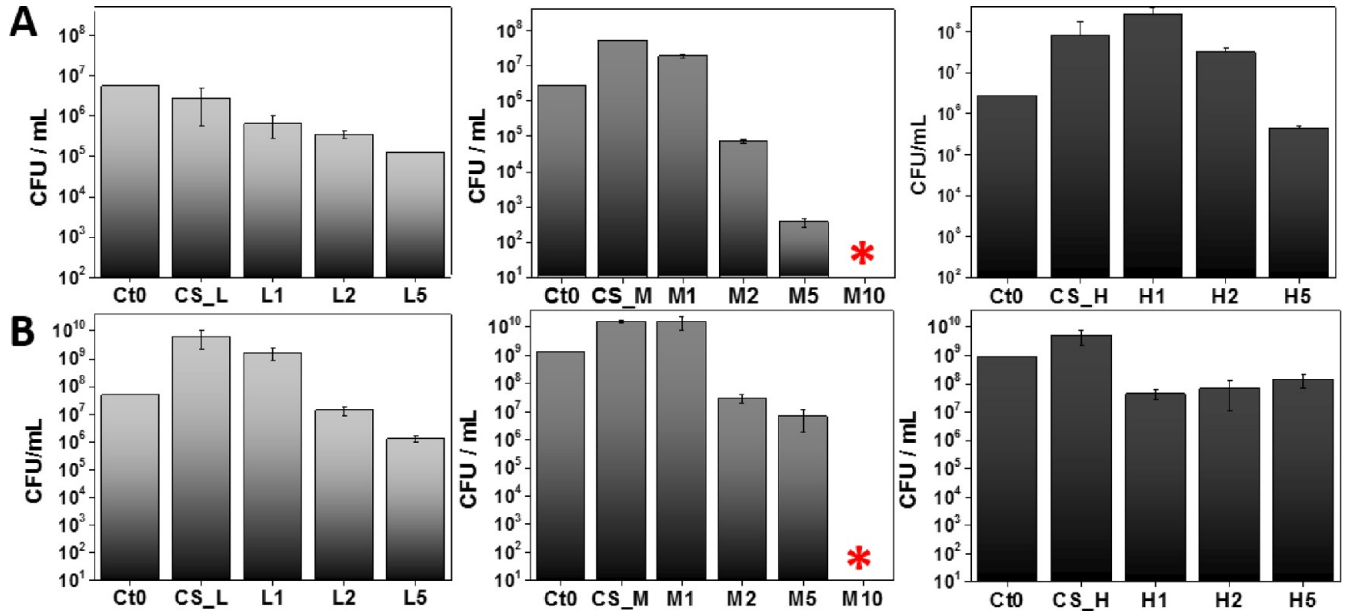

Figure 7. Antibacterial test results (Standard Norm ASTM E2180-07) for CS_L/M/H composites with different based AuNPs loading (1, 2, 5 and 10 mM gold precursor), against *S. aureus* ATCC 25923 (A) and *P. aeruginosa* ATCC 27853 (B). Data were expressed as the mean ± standard error (n = 3).

corresponding to amide I groups, C−O stretching along with N−H deformation mode (acetylated amine, and to free amine groups, respectively).[54] Absorption at 1376 and 1409 cm^{-1} could be assigned to bending vibrations of $-CH_2$ and $-CH_3$, respectively.[60] Also, 1320 and 1259 cm^{-1} bands can be distinguished, corresponding, respectively, to CH_2 wagging vibration in primary alcohol and the amide III vibration coming from combination of N−H deformation and C−N stretching.

The most representative changes coming from metal−chitosan interactions occur for the amino group band (~1590 cm^{-1} for pure polymer), which shifts to lower wavenumbers in the presence of gold nanoparticles due to electrostatic interactions between the polymer and the NPs. The spectra clearly determine the interactions between the primary amino groups with the metal nanoparticle surfaces.[61,62] Similar results were previously obtained for chitosan−silver by Wei et al. and Potara et al.[48,63]

XPS Results. Figure 6A presents the Au/C atomic ratio course upon different ion bombardment times for chitosan M films with two of the highest gold contents (M5 and M10). The low gold values observed on the surface could be due to the absence of gold nanoparticles on the surface, but it could also be produced by the unavoidable atmospheric contamination consisting mainly of carbon and oxygen. Another explanation for the low gold surface concentration could be the XPS analysis conditions, the samples are dried at very low pressure and it could cause the shrinking of the polymer chains on the surface encapsulating the gold nanoparticles. After etching, a few layers of the film were removed on sample M5 (≈20 nm) and the gold concentration remained constant, indicating a proper dispersion of the nanoparticles along the film depth. According to the Au/C ratio values for the M10 sample, the thickness showing a gold gradient concentration is thicker, around 80 nm. XPS maps of the surface of the films show a homogeneous gold nanoparticle distribution in both samples (Figure 6B,C).

Antibacterial Activity Test. To determine the biocidal potential of CS-AuNP films, two representative bacterial strains were selected. Both of them, *S. aureus* ATTC 25923 and *P. aeruginosa* ATTC 27853, normally populate the skin or mucous

DOI: 10.1021/am508094e
ACS Appl. Mater. Interfaces 2015, 7, 1087−1099

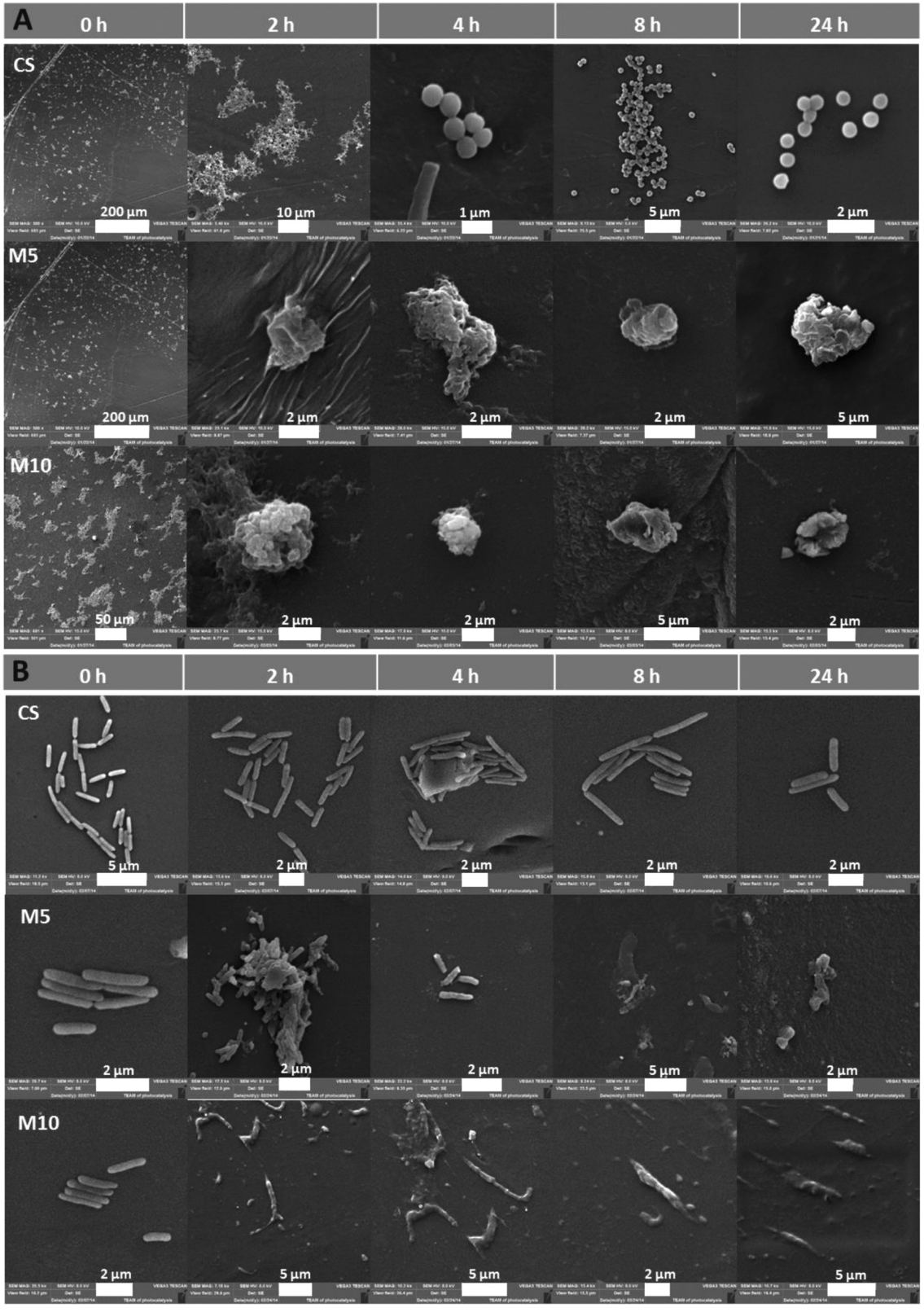

Figure 8. SEM micrographs representing the morphology of the bacteria cell wall upon contact with chitosan and chitosan−gold nanocomposites (CS_M with 5 and 10 mM gold initial precursor) on (A) *S. aureus* ATTC 25923 and (B) *P. aeruginosa* ATCC 27853.

membranes of humans and cause a wide range of serious diseases.[64,65] The antibacterial activity of gold nanoparticles embedded within the chitosan films was tested according to the Standard Norm ASTM E2180-07 for polymeric substances. Composites were sterilized before the antibacterial test, according to the norm demands. To certify the reproducibility of antibacterial tests, experiments were performed in triplicate. The test results were calculated as CFU/mL and are presented

DOI: 10.1021/am508094e
ACS Appl. Mater. Interfaces 2015, 7, 1087−1099

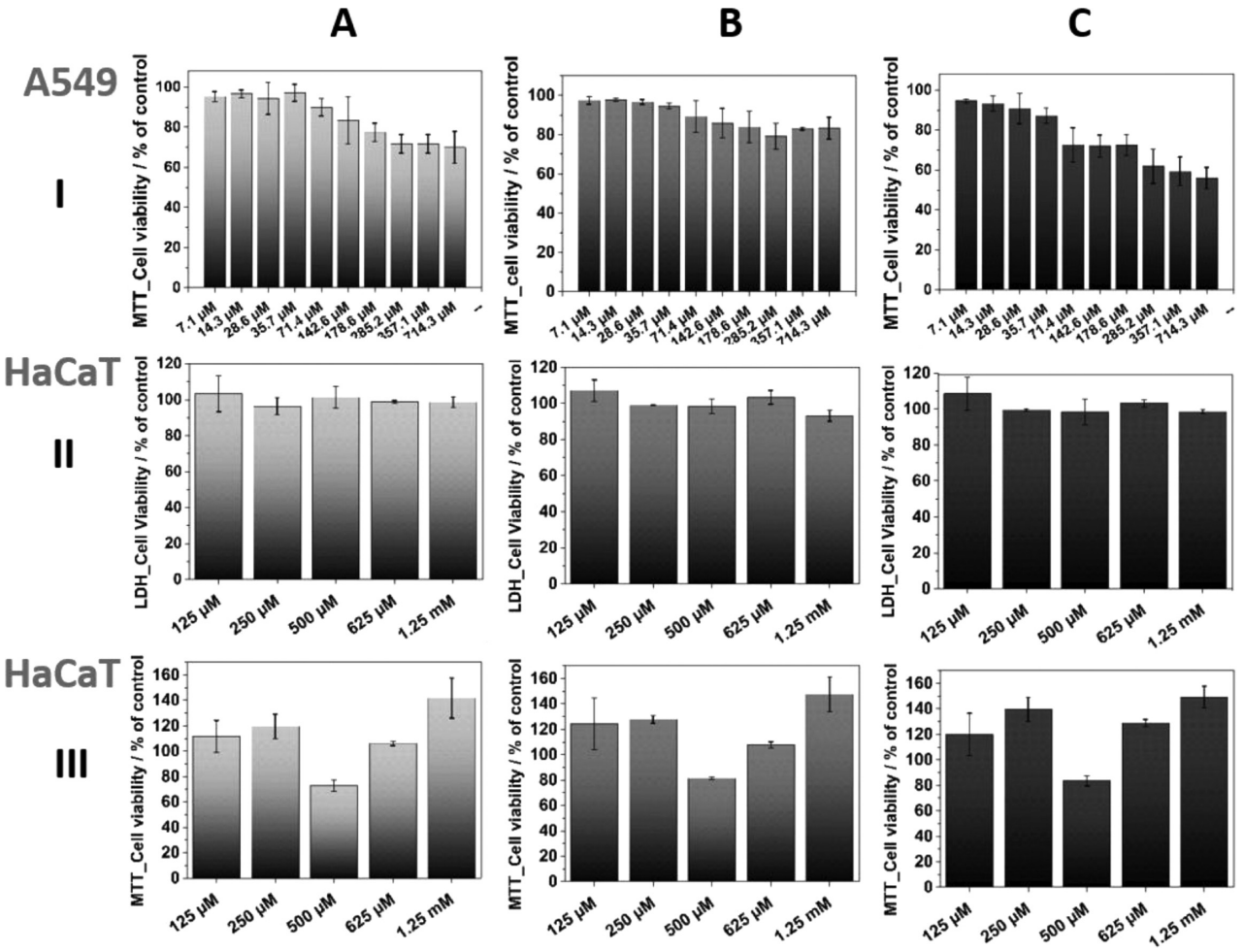

Figure 9. Cellular viability after incubation with different CS_L (A), CS_M (B), CS_H (C) based AuNP colloid concentrations for A549 (I, MTT assay) and HaCaT (II, LDH assay; III, MTT assay) cell line. Data are expressed as the mean ± standard error (n = 9).

in Figure 7 (Ct_0 stands for initial bacterial culture at the beginning of the experiment).

Films based on chitosan with medium Mw and one of the uppermost gold content (M5) demonstrated the highest antibacterial effect in comparison to chitosan with low and high Mw based composites. Gram-negative biofilm forming strains (*P. aeruginosa*) appeared to be more resistant than Gram-positive *S. aureus* at each gold nanoparticle concentration. Based on these results, CS_M was selected for the preparation of nanocomposites with the highest AuNP content, M10. A total bactericidal effect for those materials was obtained (Figure 7*). The molecular weight of chitosan clearly affects the antibacterial activity of the resulting nanocomposites. The biocidal effect was reduced for materials based on CS_H, intermediate for CS_L and finally the most effective antimicrobial material appeared to be CS_M. Additionally, SEM analysis was carried out in order to evaluate the morphological changes in the bacterial cell wall upon contact with the bactericidal films (M5 and M10). Bacterial cell structural damage, induced by CS-AuNPs, was clearly observed for both tested strains (Figure 8). Multiple holes and perforations were formed on the surface of *S. aureus* after exposure to M5 and M10 films, resulting in a total cell disintegration. Similarly, *P. aeruginosa* cells seem to alter their form, from elongated bacillus to ragged and irregular shapes, which confirms their total lysis. Results stay in agreement with the obtained CFU values. The presented characteristics of the prepared nanocomposites enable to analyze and understand their biological activity more accurately. Several reports concerning the mechanism of chitosan or gold nanoparticles antibacterial activity have been presented.[49,57] However, the exact mechanisms have not been elucidated yet. Other authors demonstrate that polycationic chitosan interacts with negatively charged bacterial cell wall and leads to intracellular components leakage.[66] The higher DD and amino groups number, the higher positive charge enabling interactions with cell wall and finally, the better antibacterial potential of pure polymeric films.[67] Also, low molecular weight of the polymer facilitates cell wall penetration and interaction with intracellular components whereas high Mw enables only surface interactions.[68] Here, the main bactericidal effect is a result of the AuNPs activity, which is also an object of many scientific papers trying to explain their mechanism. AuNPs can interact with sulfur-containing proteins in the cell membrane changing its permeability, leading to intracellular components leakage and finally cell death or/and bind to DNA and inhibit transcription.[69] As the positive charge of the polymer is greatly reduced upon AuNP synthesis and further film formation, the antibacterial activity of chitosan films decreases in comparison to the polymeric dispersion. Still, bacteriostatic activity of chitosan films can be observed. It has been shown that size and AuNP dispersion degree influence their antimicrobial activity.

DOI: 10.1021/am508094e
ACS Appl. Mater. Interfaces 2015, 7, 1087−1099

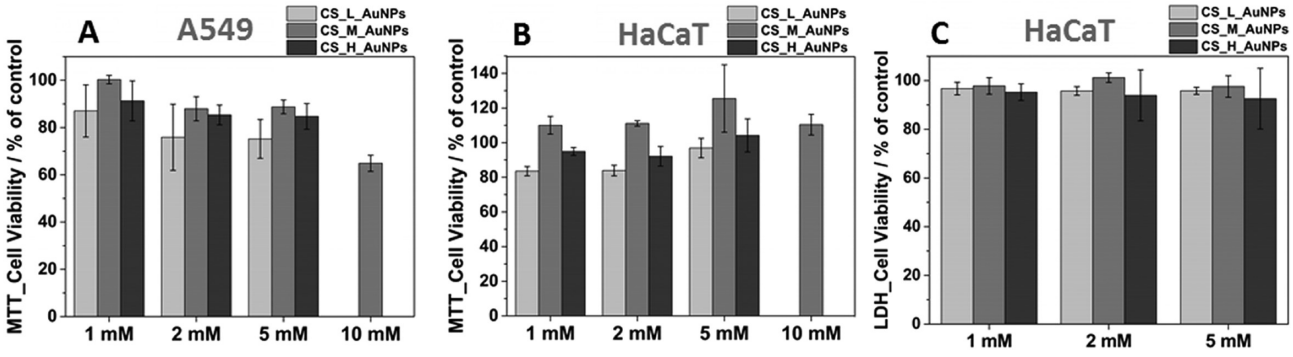

Figure 10. Cellular viability after 24 h incubation with CS L/M/H based nanocomposites with different content of gold nanoparticles A549 (A) MTT assay and HaCaT (B) MTT and (C) LDH assay. Data are expressed as the mean ± standard error (n = 9).

The smaller and well-distributed gold nanoparticles, the more significant bacteria depletion occurs. Chitosan with medium Mw appears to be the best stabilizing agent for AuNP formation. The obtained gold nanoparticles have the smallest size and the most uniform distribution across the resulting films when using this medium Mw chitosan. Thanks to the high DD and thus the high number of amino groups responsible for NPs formation, a high reduction rate for the gold ions is also obtained.[70] Because the reduction and seed formation occur in many places at once, the smallest nanoparticles are formed compared to the other Mw chitosans tested. As the viscosity of the polymer increases, the formation of less nucleation centers is more probable due to the hindered ion diffusion and reducing agent across the gel. The molecular weight of the polymer influences also further AuNP distribution in the resulting film. Low and high Mw polymers do not ensure good NP distribution across the film due to their insufficient stabilization and thus diffusion or aggregates formation, respectively. Our results stay in agreement with previous work of Prema et al. and Zhang et al., who presented chitosan and other polysaccharide stabilized gold nanoparticles as antibacterial agents.[57,71] Bacterial cell wall morphology upon incubation with chitosan medium based nanocomposites was further analyzed, and the results support their bactericidal action (Figure 8). For both bacterial strains tested, significant and progressive damage on the cell wall can be observed, which resulted in total cell lysis. Another important aspect that we present is the importance of a direct contact between materials and bacteria in order to achieve bactericidal effect. Even when the XPS results showed a low gold concentration on the surface, during the bactericidal test swelling of the polymer would occur, allowing the contact of AuNP with the bacteria. We confirmed the absence of AuNP detachment from the prepared nanocomposites by UV−vis spectrophotometry. Those results importantly contribute to the cytotoxicity test outcomes explanation.

Cytotoxicity Assay. MTT and LDH assays were carried out to assess the effect of chitosan−gold nanocomposites on mammalian cell viability. Any possible interference of the nanoparticles with the colorimetric tests was discarded.[72] The cytotoxicity of the prepared materials was evaluated after 24 h of incubation for both colloids based on gold nanoparticles embedded in chitosan and solid nanocomposites. Figure 9 presents the data for A549 cells, showing a slight and concentration-dependent decrease in cell viability assessed by the MTT test. Increasing in the range from 143 μM up to 714 μM, the most significant cytotoxic effect can be observed for AuNPs based on chitosan with the highest Mw, where the cell population reduction reaches almost a 45%. Similarly, for CS_L based samples, cellular viability decreased to a 69% for the highest concentration tested. The lowest cell population reduction (<18%) is observed for chitosan with the medium Mw.

Noteworthy, a wide concentration range remains at very high micromolar levels without a significant cytotoxic effect, which is a remarkable novelty. A similar effect was observed for HaCaT cells, where no acute cytotoxicity was noted for almost all AuNPs concentrations. Cytotoxicity of CS-AuNPs colloids was tested to present that even the possibility of direct internalization of chitosan modified gold nanoparticles into cells do not cause acute viability reduction up to micromolar concentrations. Figure 9II and III shows both LDH and MTT assay results after 24 h of incubation. According to the MTT test, only the 500 μM AuNP seem to cause diminution of cell population, whereas LDH assay indicated no cytotoxic effect.

In the next step, A549 and HaCaT cells were incubated with chitosan−gold nanocomposites after 24 h. Again, the cytotoxicity was quantified by the MTT and LDH assays (Figure 10). Concentration of AuNPs and chitosan molecular weight clearly influence the toxic effect for both cell lines. According to the MTT results, CS_L based films at each AuNPs concentration level exhibited the highest reduction rate (~20%) for both cell lines. However, A549 cells appeared to be more sensitive to the nanocomposite presence and the M10 sample induced almost 40% viability reduction (Figure 10A). Still, CS_M samples with lower gold content were the least toxic. Importantly, HaCaT cells turned out to be more tolerant to CS-AuNPs contact (Figure 10B,C). No cell viability reduction was noted even for the M10 composite. Additionally, LDH test was performed for HaCaT cells and confirms no significant cytotoxicity on the tested materials.

The wide interest in AuNP containing materials, coming from a broad variety of outstanding properties, forces scientists to evaluate and explain their possible cytotoxic effects. Generally, gold nanoparticles are described as chemically stable, biocompatible and nontoxic.[39] The amount of data about possible AuNP−cell interactions is successively increasing. Simon and Jahnen-Dechent reported that 1−2 nm AuNPs were highly toxic, irrespective to the cell type tested, whereas colloidal forms of larger 15 nm NPs were comparatively nontoxic.[37] Effect of size, concentration and exposure time for AuNPs toxicity in the case of human dermal fibroblast was evaluated by Miranova et al.[36] Different mechanisms of AuNPs cellular uptake was discovered, depending on their size.

DOI: 10.1021/am508094e
ACS Appl. Mater. Interfaces 2015, 7, 1087−1099

Importantly, AuNPs induced cell damage is not permanent, meaning that the cells have the ability to recover. On the other hand, Li et al. provided evidence that 20 nm AuNP treatment could generate oxidative stress in MRC-5 lung fibroblasts.[73] Cytotoxicity test results for colloidal AuNPs in chitosan with medium Mw demonstrate almost no changes in cell viability after 24 h of incubation up to 700 μM concentration for A549 and even with 1 mM for HaCaT cell lines, in agreement with previously reported colloidal forms of AuNPs with lack of toxicity up to 6300 μM.[37] Another aspect is the nanoparticle surface modification with polymers. It has been demonstrated that the cytotoxic effect can be greatly reduced by using PAA-, PAH-, PMA-, PEG-coated gold nanorods (NRDs) in nanomolar concentrations.[40] Also, biopolymeric coatings as proteins, e.g., transferrin, can greatly reduce cytotoxic effect.[74] Herein, no significant cytotoxicity of resulting nanocomposites might be a consequence of biocompatible chitosan layer surrounding the AuNP surface. Due to the presence of chemical bonds between AuNPs and chitosan, the potential direct interactions of bare nanoparticles with cellular components might be weakened. Lack of AuNP release from the nanocomposites supports the biocompatible character of those materials. Moreover, the average diameter of AuNPs synthesized with three different chitosans is higher than 10 nm, which are reported to be less toxic.[37]

Previously, we reported chitosan impregnated with silver NP as composites exhibiting total bactericidal effect against resistant and biofilm forming strains of *S. aureus*.[54] Silver nanoparticle cytotoxic effects are widely described in the literature. Reversely, chitosan−gold nanocomposites show antimicrobial action and no toxicity against human cells at the doses tested, which makes them a perfect candidate for many biomedical applications including wound dressings, adhesive bandages, coatings, etc.

4. CONCLUSIONS

We have reported herein the synthesis of chitosan based gold nanoparticles and further innovative nanocomposite preparation. The main goal of the presented study was to optimize the procedure of chitosan based AuNP synthesis and films preparation in order to obtain materials with high antibacterial activity and simultaneously low cytotoxicity. Application of three different chitosan grades varying the average molecular weight and the deacetylation degree enabled us to reveal Mw/DD AuNP properties dependency. Gold nanoparticles based on chitosan with medium Mw and the highest DD exhibited the smallest average diameter (~15 nm). The resulting nanocomposites demonstrated total bactericidal effect against two biofilm forming antibiotic resistant strains (*S. aureus* and *P. aeruginosa*). Homogenous AuNP distribution in CS_M films and strong nanoparticle attachment to the polymer was shown. Importantly, Au size in the range between 10 and 20 nm resulted in no significant cytotoxic effects on human cells. The polymeric layer on the NP surface also might be a reason for reduced toxic effects or even total toxicity exclusion.

■ ASSOCIATED CONTENT

Supporting Information

Description of antibacterial test procedure, bacterial cell wall damage SEM visualization and composites physicochemical characterization details. This material is available free of charge via the Internet at http://pubs.acs.org.

■ AUTHOR INFORMATION

Corresponding Authors

*M. Kus-Liśkiewicz. Phone: +48178723708. E-mail: mkus@univ.rzeszow.pl.

*M. Arruebo. Phone: +34 876 555437. E-mail: arruebom@unizar.es.

*A. Kyzioł. Phone: +4812 6632221. E-mail: kyziol@chemia.uj.edu.pl.

Notes

The authors declare no competing financial interest.

■ ACKNOWLEDGMENTS

The authors are grateful to Dr. Olexandr Korchynskyi and Prof. Mykhailo Gonchar for enabling experiments on the HaCaT cell line. IDEAS PLUS (No. IdP2012000362) and ATOMIN (POIG.02.01.00-12-023/08) projects are gratefully acknowledged. Financial support from the EU thanks to the ERC Consolidator Grant program (ERC-2013-CoG-614715, NANOHEDONISM) is gratefully acknowledged.

■ REFERENCES

(1) Joint Technical Report the Bacterial Challenge: Time to React. European Centre for Disease Prevention and Control/European Medicines Agency. http://www.ecdc.europa.eu/en/publications/Publications/0909_TER_The_Bacterial_Challenge_Time_to_React.pdf, 2009.

(2) WHO Antimicrobial Resistance. http://www.who.int/mediacentre/factsheets/fs194/en/, 2014.

(3) WHO. http://www.stoptb.org/Wg/Mdrtb/, 2014.

(4) Rai, M.; Yadav, A.; Gade, A. Silver Nanoparticles as a New Generation of Antimicrobials. *Biotechnol. Adv.* **2009**, *27*, 76−83.

(5) Pal, S.; Tak, Y. K.; Song, J. M. Does the Antibacterial Activity of Silver Nanoparticles Depend on the Shape of the Nanoparticle? A Study of the Gram-Negative Bacterium *Escherichia coli*. *Appl. Environ. Microbiol.* **2007**, *73*, 1712−1720.

(6) Cioffi, N.; Torsi, L.; Ditaranto, N.; Tantillo, G.; Ghibelli, L.; Sabbatini, L.; Bleve-Zacheo, T.; D'Alessio, M.; Zambonin, P. G.; Traversa, E. Copper Nanoparticle/Polymer Composites with Antifungal and Bacteriostatic Properties. *Chem. Mater.* **2005**, *17*, 5255−5262.

(7) Chamundeeswari, M.; Sobhana, S. S. L.; Jacob, J. P.; Kumar, M. G.; Devi, M. P.; Sastry, T. P.; Mandal, A. B. Preparation, Characterization and Evaluation of a Biopolymeric Gold Nanocomposite with Antimicrobial Activity. *Biotechnol. Appl. Biochem.* **2010**, *55*, 29−35.

(8) Foldbjerg, R.; Dang, D.; Autrup, H. Cytotoxicity and Genotoxicity of Silver Nanoparticles in the Human Lung Cancer Cell Line, A549. *Arch. Toxicol.* **2011**, *85*, 743−750.

(9) Nowack, B.; Krug, H. F.; Height, M. 120 Years of Nanosilver History: Implications for Policy Makers. *Environ. Sci. Technol.* **2011**, *45*, 1177−1183.

(10) Suliman Y, A. O.; Ali, D.; Alarifi, S.; Harrath, A. H.; Mansour, L.; Alwasel, S. H. Evaluation of Cytotoxic, Oxidative Stress, Proinflammatory and Genotoxic Effect of Silver Nanoparticles in Human Lung Epithelial Cells. *Environ. Toxicol.* **2013**, DOI: 10.1002/tox.21880.

(11) Jose, G.; Santra, S.; Mandal, S.; Sengupta, T. Singlet Oxygen Mediated DNA Degradation by Copper Nanoparticles: Potential Towards Cytotoxic Effect on Cancer Cells. *J. Nanobiotechnol.* **2011**, *9*, 1−8.

(12) Song, L.; Connolly, M.; Fernández-Cruz, M. L.; Vijver, M. G.; Fernández, M.; Conde, E.; de Snoo, G. R.; Peijnenburg, W. J. G. M.; Navas, J. M. Species-Specific Toxicity of Copper Nanoparticles among Mammalian and Piscine Cell Lines. *Nanotoxicology* **2013**, *8*, 383−393.

(13) Bergen, J. M.; von Recum, H. A.; Goodman, T. T.; Massey, A. P.; Pun, S. H. Gold Nanoparticles as a Versatile Platform for

DOI: 10.1021/am508094e
ACS Appl. Mater. Interfaces 2015, 7, 1087−1099

Optimizing Physicochemical Parameters for Targeted Drug Delivery. *Macromol. Biosci.* **2006**, *6*, 506−516.
(14) Boisselier, E.; Astruc, D. Gold Nanoparticles in Nanomedicine: Preparations, Imaging, Diagnostics, Therapies and Toxicity. *Chem. Soc. Rev.* **2009**, *38*, 1759−1782.
(15) Ghosh, P.; Han, G.; De, M.; Kim, C. K.; Rotello, V. M. Gold Nanoparticles in Delivery Applications. *Adv. Drug Delivery Rev.* **2008**, *60*, 1307−1315.
(16) Jain, P. K.; El-Sayed, I. H.; El-Sayed, M. A. Au Nanoparticles Target Cancer. *Nano Today* **2007**, *2*, 18−29.
(17) Pissuwan, D.; Valenzuela, S. M.; Cortie, M. B. Therapeutic Possibilities of Plasmonically Heated Gold Nanoparticles. *Trends Biotechnol.* **2006**, *24*, 62−67.
(18) Zhou, Y.; Kong, Y.; Kundu, S.; Cirillo, J.; Liang, H. Antibacterial Activities of Gold and Silver Nanoparticles against *Escherichia coli* and Bacillus Calmette-Guérin. *J. Nanobiotechnol.* **2012**, *10*, 1−9.
(19) Pissuwan, D.; Cortie, C. H.; Valenzuela, S. M.; Cortie, M. B. Functionalised Gold Nanoparticles for Controlling Pathogenic Bacteria. *Trends Biotechnol.* **2010**, *28*, 207−213.
(20) Badwaik, V.; Vangala, L.; Pender, D.; Willis, C.; Aguilar, Z.; Gonzalez, M.; Paripelly, R.; Dakshinamurthy, R. Size-Dependent Antimicrobial Properties of Sugar-Encapsulated Gold Nanoparticles Synthesized by a Green Method. *Nanoscale Res. Lett.* **2012**, *7*, 623.
(21) Zhang, W.; Li, Y.; Niu, J.; Chen, Y. Photogeneration of Reactive Oxygen Species on Uncoated Silver, Gold, Nickel, and Silicon Nanoparticles and Their Antibacterial Effects. *Langmuir* **2013**, *29*, 4647−4651.
(22) Cui, Y.; Zhao, Y.; Tian, Y.; Zhang, W.; Lü, X.; Jiang, X. The Molecular Mechanism of Action of Bactericidal Gold Nanoparticles on *Escherichia coli*. *Biomaterials* **2012**, *33*, 2327−2333.
(23) Norman, R. S.; Stone, J. W.; Gole, A.; Murphy, C. J.; Sabo-Attwood, T. L. Targeted Photothermal Lysis of the Pathogenic Bacteria, *Pseudomonas aeruginosa*, with Gold Nanorods. *Nano Lett.* **2007**, *8*, 302−306.
(24) Perni, S.; Prokopovich, P.; Pratten, J.; Parkin, I. P.; Wilson, M. Nanoparticles: Their Potential Use in Antibacterial Photodynamic Therapy. *Photochem. Photobiol. Sci.* **2011**, *10*, 712−720.
(25) Shukla, R.; Bansal, V.; Chaudhary, M.; Basu, A.; Bhonde, R. R.; Sastry, M. Biocompatibility of Gold Nanoparticles and Their Endocytotic Fate inside the Cellular Compartment: A Microscopic Overview. *Langmuir* **2005**, *21*, 10644−10654.
(26) Paino, I. M. M.; Marangoni, V. S.; de Oliveira, R. d. C. S.; Antunes, L. M. G.; Zucolotto, V. Cyto and Genotoxicity of Gold Nanoparticles in Human Hepatocellular Carcinoma and Peripheral Blood Mononuclear Cells. *Toxicol. Lett.* **2012**, *215*, 119−125.
(27) Goodman, C. M.; McCusker, C. D.; Yilmaz, T.; Rotello, V. M. Toxicity of Gold Nanoparticles Functionalized with Cationic and Anionic Side Chains. *Bioconjugate Chem.* **2004**, *15*, 897−900.
(28) Tarantola, M.; Pietuch, A.; Schneider, D.; Rother, J.; Sunnick, E.; Rosman, C.; Pierrat, S.; Sönnichsen, C.; Wegener, J.; Janshoff, A. Toxicity of Gold-Nanoparticles: Synergistic Effects of Shape and Surface Functionalization on Micromotility of Epithelial Cells. *Nanotoxicology* **2011**, *5*, 254−268.
(29) Kroll, A.; Pillukat, M.; Hahn, D.; Schnekenburger, J. Interference of Engineered Nanoparticles with in Vitro Toxicity Assays. *Arch. Toxicol.* **2012**, *86*, 1123−1136.
(30) Ong, K. J.; MacCormack, T. J.; Clark, R. J.; Ede, J. D.; Ortega, V. A.; Felix, L. C.; Dang, M. K. M.; Ma, G.; Fenniri, H.; Veinot, J. G. C.; Goss, G. G. Widespread Nanoparticle-Assay Interference: Implications for Nanotoxicity Testing. *PLoS One* **2014**, *9*, e90650.
(31) Coulter, J. A.; Jain, S.; Butterworth, K. T.; Taggart, L. E.; Dickson, G. R.; McMahon, S. J.; Hyland, W. B.; Muir, M. F.; Trainor, C.; Hounsell, A. R.; O'Sullivan, J. M.; Schettino, G.; Currell, F. J.; Hirst, D. G.; Prise, K. M. Cell Type-Dependent Uptake, Localization, and Cytotoxicity of 1.9 nm Gold Nanoparticles. *Int. J. Nanomed.* **2012**, *7*, 2673−2685.
(32) Chithrani, B. D.; Ghazani, A. A.; Chan, W. C. W. Determining the Size and Shape Dependence of Gold Nanoparticle Uptake into Mammalian Cells. *Nano Lett.* **2006**, *6*, 662−668.
(33) Coradeghini, R.; Gioria, S.; García, C. P.; Nativo, P.; Franchini, F.; Gilliland, D.; Ponti, J.; Rossi, F. Size-Dependent Toxicity and Cell Interaction Mechanisms of Gold Nanoparticles on Mouse Fibroblasts. *Toxicol. Lett.* **2013**, *217*, 205−216.
(34) Soenen, S. J.; Manshian, B.; Montenegro, J. M.; Amin, F.; Meermann, B.; Thiron, T.; Cornelissen, M.; Vanhaecke, F.; Doak, S.; Parak, W. J.; De Smedt, S.; Braeckmans, K. Cytotoxic Effects of Gold Nanoparticles: A Multiparametric Study. *ACS Nano* **2012**, *6*, 5767−5783.
(35) Gao, W.; Xu, K.; Ji, L.; Tang, B. Effect of Gold Nanoparticles on Glutathione Depletion-Induced Hydrogen Peroxide Generation and Apoptosis in Hl7702 Cells. *Toxicol. Lett.* **2011**, *205*, 86−95.
(36) Mironova, T.; Hadjiargyrou, M.; Simon, M.; Jurkovski, V.; Railovich, M. H. Gold Nanoparticles Cellular Toxicity and Recovery: Effect of Size, Concentration and Exposure Time. *Nanotoxicology* **2010**, *4*, 120−137.
(37) Pan, Y.; Neuss, S.; Leifert, A.; Fischler, M.; Wen, F.; Simon, U.; Schmid, G.; Brandau, W.; Jahnen-Dechent, W. Size-Dependent Cytotoxicity of Gold Nanoparticles. *Small* **2007**, *3*, 1941−1949.
(38) Hondroulis, E.; Liu, C.; Li, C.-Z. Whole Cell based Electrical Impedance Sensing Approach for a Rapid Nanotoxicity Assay. *Nanotechnology* **2010**, *21*, 315103.
(39) Connor, E. E.; Mwamuka, J.; Gole, A.; Murphy, C. J.; Wyatt, M. D. Gold Nanoparticles Are Taken up by Human Cells but Do Not Cause Acute Cytotoxicity. *Small* **2005**, *1*, 325−327.
(40) Alkilany, A. M.; Nagaria, P. K.; Hexel, C. R.; Shaw, T. J.; Murphy, C. J.; Wyatt, M. D. Cellular Uptake and Cytotoxicity of Gold Nanorods: Molecular Origin of Cytotoxicity and Surface Effects. *Small* **2009**, *5*, 701−708.
(41) Qiu, Y.; Liu, Y.; Wang, L.; Xu, L.; Bai, R.; Ji, Y.; Wu, X.; Zhao, Y.; Li, Y.; Chen, C. Surface Chemistry and Aspect Ratio Mediated Cellular Uptake of Au Nanorods. *Biomaterials* **2010**, *31*, 7606−7619.
(42) Jokerst, J. V.; Lobovkina, T.; Zare, R. N.; Gambhir, S. S. Nanoparticle PEGylation for Imaging and Therapy. *Nanomedicine* **2011**, *6*, 715−728.
(43) Niidome, T.; Yamagata, M.; Okamoto, Y.; Akiyama, Y.; Takahashi, H.; Kawano, T.; Katayama, Y.; Niidome, Y. PEG-Modified Gold Nanorods with a Stealth Character for in Vivo Applications. *J. Controlled Release* **2006**, *114*, 343−347.
(44) Vijayakumar, S.; Ganesan, S. In Vitro Cytotoxicity Assay on Gold Nanoparticles with Different Stabilizing Agents. *J. Nanomaterials* **2012**, *2012*, 14−14.
(45) Rhim, J.-W.; Hong, S.-I.; Park, H.-M.; Ng, P. K. W. Preparation and Characterization of Chitosan-based Nanocomposite Films with Antimicrobial Activity. *J. Agric. Food. Chem.* **2006**, *54*, 5814−5822.
(46) Amin, K. A. M.; Panhuis, M. Reinforced Materials Based on Chitosan, TiO_2 and Ag Composites. *Polymers* **2012**, *4*, 590−599.
(47) Dongwei, W.; Wuyong, S.; Weiping, Q.; Yongzhong, Y.; Xiaoyuan, M. The Synthesis of Chitosan-based Silver Nanoparticles and Their Antibacterial Activity. *Carbohydr. Res.* **2009**, *344*, 2375−2382.
(48) Wei, D.; Qian, W. Facile Synthesis of Ag and Au Nanoparticles Utilizing Chitosan as a Mediator Agent. *Colloids Surf., B* **2008**, *62*, 136−142.
(49) Kong, M.; Chen, X. G.; Xing, K.; Park, H. J. Antimicrobial Properties of Chitosan and Mode of Action: A State of the Art Review. *Int. J. Food Microbiol.* **2010**, *144*, 51−63.
(50) Ralston, G. B.; Tracey, M. V.; Wrench, P. M. Inhibition of Fermentation in Bakers Yeast by Chitosan. *Biochim. Biophys. Acta* **1964**, *93*, 653.
(51) Fang, S. W.; Li, C. F.; Shih, D. Y. C. Antifungal Activity of Chitosan and Its Preservative Effect on Low-Sugar Candied Kumquat. *J. Food Prot.* **1994**, *57*, 136−140.
(52) Raafat, D.; Sahl, H. G. Chitosan and Its Antimicrobial Potential - A Critical Literature Survey. *Microb. Biotechnol.* **2009**, *2*, 186−201.
(53) ASTM International. *Standard Test Method for Determining the Activity of Incorporated Antimicrobial Agent(s) in Polymeric or Hydrophobic Materials*; ASTM Standard E2180-07; ASTM International: West Conshohocken, PA, 2007.

DOI: 10.1021/am508094e
ACS Appl. Mater. Interfaces 2015, 7, 1087−1099

(54) Regiel, A.; Irusta, S.; Kyzioł, A.; Arruebo, M.; Santamaria, J. Preparation and Characterization of Chitosan-Silver Nanocomposite Films and Their Antibacterial Activity against *Staphylococcus aureus*. *Nanotechnology* **2013**, *24*, 015101.
(55) Chan, F. K.-M.; Moriwaki, K.; Rosa, M. J. Detection of Necrosis by Release of Lactate Dehydrogenase Activity. *Immune Homeostasis* **2013**, *979*, 65−70.
(56) Potara, M.; Maniu, D.; Astilean, S. The Synthesis of Biocompatible and SERS-Active Gold Nanoparticles Using Chitosan. *Nanotechnology* **2009**, *20*, 315602.
(57) Prema, P.; Thangaoandiyan, S. In-Vitro Antibacterial Activity of Gold Nanoparticles Capped with Polysaccharide Stabilizing Agents. *Int. J. Pharm. Pharm. Sci.* **2013**, *5*, 310−314.
(58) Haiss, W.; Thanh, N. T. K.; Aveyard, J.; Fernig, D. G. Determination of Size and Concentration of Gold Nanoparticles from UV−vis Spectra. *Anal. Chem.* **2007**, *79*, 4215−4221.
(59) Sau, T.; Pal, A.; Jana, N. R.; Wang, Z. L.; Pal, T. Size Controlled Synthesis of Gold Nanoparticles Using Photochemically Prepared Seed Particles. *J. Nanopart. Res.* **2001**, *3*, 257−261.
(60) Salcedo, I.; Sandri, G.; Aguzzi, C.; Bonferoni, C.; Cerezo, P.; Sánchez-Espejo, R.; Viseras, C. Intestinal Permeability of Oxytetracycline from Chitosan-Montmorillonite Nanocomposites. *Colloids Surf., B* **2014**, *117*, 441−448.
(61) Devi, R.; Yadav, S.; Nehra, R.; Yadav, S.; Pundir, C. S. Electrochemical Biosensor Based on Gold Coated Iron Nanoparticles/Chitosan Composite Bound Xanthine Oxidase for Detection of Xanthine in Fish Meat. *J. Food Eng.* **2013**, *115*, 207−214.
(62) Potara, M. Designing New Chitosan-Coated Plasmonic NPs for Biomolecular Sensing and Antibacterial Activity. Doctoral Thesis Summary, 2012.
(63) Potara, M.; Jakab, E.; Damert, A.; Popescu, O.; Canpean, V.; Astilean, S. Synergistic Antibacterial Activity of Chitosan−Silver Nanocomposites on *Staphylococcus aureus*. *Nanotechnology* **2011**, *22*, 135101.
(64) Lowy, F. D. *Staphylococcus aureus* Infections. *N. Engl. J. Med.* **1998**, *339*, 520−532.
(65) Høiby, N. Recent Advances in the Treatment of *Pseudomonas aeruginosa* Infections in Cystic Fibrosis. *BMC Med.* **2011**, *9*, 1−7.
(66) Ignatova, M.; Manolova, N.; Rashkov, I. Novel Antibacterial Fibers of Quaternized Chitosan and Poly(vinyl pyrrolidone) Prepared by Electrospinning. *Eur. Polym. J.* **2007**, *43*, 1112−1122.
(67) Jung, E. J.; Youn, D. K.; Lee, S. H.; No, H. K.; Ha, J. G.; Prinyawiwatkul, W. Antibacterial Activity of Chitosans with Different Degrees of Deacetylation and Viscosities. *Int. J. Food Sci. Technol.* **2010**, *45*, 676−682.
(68) No, H. K.; Young Park, N.; Ho Lee, S.; Meyers, S. P. Antibacterial Activity of Chitosans and Chitosan Oligomers with Different Molecular Weights. *Int. J. Food Microbiol.* **2002**, *74*, 65−72.
(69) Rai, A.; Prabhune, A.; Perry, C. C. Antibiotic Mediated Synthesis of Gold Nanoparticles with Potent Antimicrobial Activity and Their Application in Antimicrobial Coatings. *J. Mater. Chem.* **2010**, *20*, 6789−6798.
(70) Lakshmi Narayanan, R.; Sivakumar, M. Preparation and Characterization of Gold Nanoparticles in Chitosan Suspension by One-Pot Chemical Reduction Method. *Nano Hybrids* **2014**, *6*, 47−57.
(71) Zhang, G.; Sun, X.; Jasinski, J.; Patel, D.; Gobin, A. M. Gold/Chitosan Nanocomposites with Specific near Infrared Absorption for Photothermal Therapy Applications. *J. Nanomaterials* **2012**, *2012*, 5−5.
(72) Kong, B.; Seog, J. H.; Graham, L. M.; Lee, S. B. Experimental Considerations on the Cytotoxicity of Nanoparticles. *Nanomedicine* **2011**, *6*, 929−941.
(73) Li, J. J.; Hartono, D.; Ong, C.-N.; Bay, B.-H.; Yung, L.-Y. L. Autophagy and Oxidative Stress Associated with Gold Nanoparticles. *Biomaterials* **2010**, *31*, 5996−6003.
(74) Chithrani, B. D.; Chan, W. C. W. Elucidating the Mechanism of Cellular Uptake and Removal of Protein-Coated Gold Nanoparticles of Different Sizes and Shapes. *Nano Lett.* **2007**, *7*, 1542−1550.

DOI: 10.1021/am508094e
ACS Appl. Mater. Interfaces 2015, 7, 1087−1099